ADVANCED FUNCTIONAL MATERIALS
www.afm-journal.de

ε-Branched Flexible Side Chain Substituted Diketopyrrolopyrrole-Containing Polymers Designed for High Hole and Electron Mobilities

A-Reum Han, Gitish K. Dutta, Junghoon Lee, Hae Rang Lee, Sang Myeon Lee, Hyungju Ahn, Tae Joo Shin, Joon Hak Oh, and Changduk Yang**

Based on the integrated consideration and engineering of both conjugated backbones and flexible side chains, solution-processable polymeric semiconductors consisting of a diketopyrrolopyrrole (DPP) backbone and a finely modulated branching side chain (ε-branched chain) are reported. The subtle change in the branching point from the backbone alters the π–π stacking and the lamellar distances between polymer backbones, which has a significant influence on the charge-transport properties and in turn the performances of field-effect transistors (FETs). In addition to their excellent electron mobilities (up to 2.25 cm^2 V^{-1} s^{-1}), ultra-high hole mobilities (up to 12.25 cm^2 V^{-1} s^{-1}) with an on/off ratio (I_{on}/I_{off}) of at least 10^6 are achieved in the FETs fabricated using the polymers. The developed polymers exhibit extraordinarily high electrical performance with both hole and electron mobilities superior to that of unipolar amorphous silicon.

1. Introduction

Due to their superior mechanical flexibility, roll-to-roll printing compatibility, and optoelectronic property tailorability, polymer-based field-effect transistors (FETs) are particularly well suited for fulfilling the near-future demand for bendable displays, e-paper, and radio frequency identification cards (RFIDs).[1] Consequently, great efforts in materials design have boosted the FET mobilities achievable from semiconducting polymers up to more than 1 cm^2 V^{-1} s^{-1}.[1,2] Furthermore, several recent papers have reported that mobility values surpassing 3 cm^2 V^{-1} s^{-1} can be obtained in state-of-the-art donor–acceptor (D–A) polymers based on diketopyrrolopyrrole (DPP). The DPP motif not only contributes to tight π–π spacing but also enhances the charge delocalization through its high level of co-planarity and quinoidal structure, being highly beneficial to charge-carrier transport through intermolecular hopping.[2a,3] Even though their stability in ambient electrochemical oxidative processes is necessary for the broad-based, high-value applications mentioned above, solution-processable polymeric semiconductors performing beyond the current levels—reliably exceeding 10 cm^2 V^{-1} s^{-1} with an on/off ratio (I_{on}/I_{off}) of at least 10^6—are the most compelling requirement for the progress of organic electronics.

Recently, we and other groups suggested the effectiveness of controlling the branching point of the side chain from the polymer backbone for tuning intermolecular self-assembly and charge-carrier mobility.[3a–c,4] Therefore, side-chain engineering can be as important as manipulating the conjugated building blocks in the backbones when designing high-performance conjugated polymers.[5] In this work, we report the substantially enhanced charge-transport characteristics of a series of DPP-based polymers showing vastly superior FET performance (hole mobilities (μ_h) of 12.25 cm^2 V^{-1} s^{-1} and $I_{on}/I_{off} \geq 10^6$ together with electron mobilities (μ_e) larger than 2 cm^2 V^{-1} s^{-1}). These have been achieved by simply modulating the side-chain branching position (i.e., replacing the commonly used 2-octyldodecyl solubilizing group as the β-branched chain of the DPP-based polymers with the 5-octylpentadecyl chain (ε-branched chain)). We also demonstrate the structure–property relationships regarding the interplay of the molecular packing and macroscopic charge-transport efficacy.

2. Results and Discussion

2.1. Synthesis and Characterization

Briefly, 5-octyl-1-pentadecyliodide as the key ε-branched side chain (ε-C_8C_{15}) was obtained from commercially available

A.-R. Han, Dr. G. K. Dutta, J. Lee, S. M. Lee, Prof. C. Yang
Department of Energy Engineering, School of Energy and Chemical Engineering
Low Dimensional Carbon Materials Center
Ulsan National Institute of Science and Technology (UNIST)
Ulsan 689–798, South Korea
E-mail: yang@unist.ac.kr
A.-R. Han, H. R. Lee, Prof. J. H. Oh
Department of Chemical Engineering
Pohang University of Science and Technology
Pohang, Gyeongbuk 790–784, South Korea
E-mail: joonhoh@postech.ac.kr
Dr. H. Ahn, Dr. T. J. Shin
Pohang Accelerator Laboratory
Pohang University of Science and Technology
Pohang, Gyeongbuk 790–784, South Korea

DOI: 10.1002/adfm.201403020

FULL PAPER

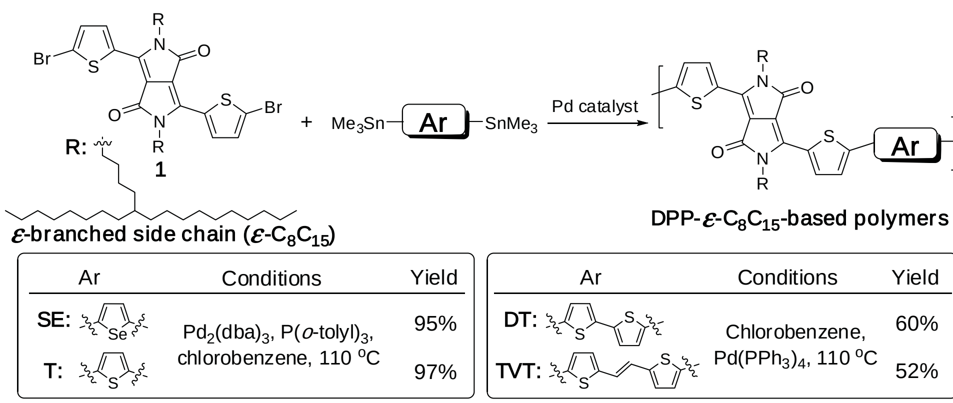

Scheme 1. Synthesis and chemical structures of DPP-based polymers bearing ε-branched side chains.

2-octyl-1-dodecanol in four steps (iodination, Grignard reaction, hydroboration-oxidation, and re-iodination).[4] The dibrominated DPP monomer (**1**) was synthesized by alkylation of the DPP core with the alkyl iodide, followed by bromination. The synthetic details and characterization data are provided in the Supporting Information (SI). In addition, the bis-stannylated co-monomers (selenophene (SE), thiophene (T), 2,2′-dithiophene (DT), and (*E*)-2-(2-(thiophen-2-yl)vinyl)thiophene (TVT)) were prepared according to the established methods.[2d,4,6] The four DPP-containing polymers (**PDPP(SE)-ε-C_8C_{15}**, **PDPP(T)-ε-C_8C_{15}**, **PDPP(DT)-ε-C_8C_{15}**, and **PDPP(TVT)-ε-C_8C_{15}** (**Scheme 1**)) were synthesized by Stille cross-coupling copolymerization of their respective bis-stannylated co-monomeric units with **1**. High-temperature (150 °C) gel-permeation chromatography (GPC) using 1,2,4-trichlorobenzene confirmed that satisfactory molecular weights (M_n = 38.2–50.8 kDa) were obtained in the cases of **PDPP(SE)-ε-C_8C_{15}** and **PDPP(T)-ε-C_8C_{15}**, whereas both **PDPP(DT)-ε-C_8C_{15}** and **PDPP(TVT)-ε-C_8C_{15}** had slightly low molecular weights (M_n < 20 kDa). This was most likely a result of their reduced solubility induced by the extending number of thiophene rings along the main backbone.

2.2. Optical and Electrochemical Properties

As shown in **Figure 1**, all the polymers exhibited strong absorptions ranging from 350 to 1100 nm in solution and as thin films (**Table 1**). Both **PDPP(SE)-ε-C_8C_{15}** and **PDPP(T)-ε-C_8C_{15}** showed marked red-shifted absorptions with broad featureless profiles when compared to **PDPP(DT)-ε-C_8C_{15}** and

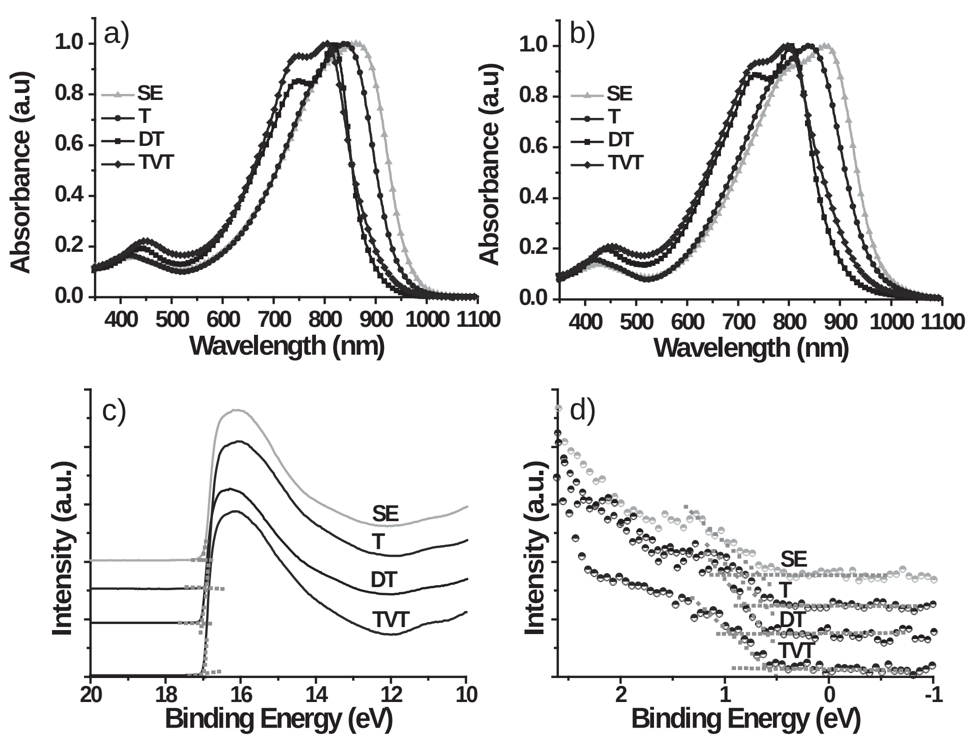

Figure 1. UV–Vis absorption spectra: a) in chloroform solution and b) as thin solid films. UPS spectra of polymer films at c) high- and d) low-energy region.

Table 1. Molecular weights, optical and electrochemical characteristics of ε-branched DPP polymers.

Polymer	M_n [kDa]/PDI	λ_{max}^{sol} [nm][a)]	λ_{max}^{film} [nm]	E_g [eV][b)]	E_{HOMO} [eV][c)]	E_{LUMO} [eV][d)]
PDPP(SE)-ε-C_8C_{15}	38.2/2.57	867	799, 870[e)]	1.26	–4.94	–3.68
PDPP(T)-ε-C_8C_{15}	50.8/2.28	840	774, 841	1.28	–4.95	–3.67
PDPP(DT)-ε-C_8C_{15}	15.4/1.95	734, 817[e)]	737, 805	1.32	–4.91	–3.59
PDPP(TVT)-ε-C_8C_{15}	19.0/2.06	745, 803	734, 797	1.35	–4.87	–3.52

[a)]Polymer solutions were prepared in chloroform with 0.5 mg mL^{-1} and the films were spin-coated on glass substrates; [b)]Determined from the onset of the electronic absorption spectra; [c)]Measured by UPS technique, incident photon energy ($h\nu$ = 21.2 eV) for He I ($E_{HOMO}^{UPS} = h\nu - (E_{cutoff} - E_{HOMO})$); [d)]$E_{LUMO} = E_{HOMO} - E_g$; [e)]Absorption maxima denote two wavelengths for absorption spectra with an additional distinguishable shoulder.

PDPP(TVT)-ε-C_8C_{15}, which both had far more pronounced vibronic structures. More interestingly, no obvious change was observed in the case of the polymers with axisymmetric donors (SE and T) upon going from solution to the solid state. This was in contrast to the polymers containing centrosymmetric units (DT and TVT), which showed slight blue shifts. These results imply that the symmetry within the polymer backbones has a significant influence on molecular conformation/organization, though the film morphologies are always accompanied by conjugation length effects. The highest occupied molecular orbital (HOMO) energy levels of all the polymers were measured by ultraviolet photoelectron spectroscopy (UPS), and the resulting HOMO values were between –4.95 eV and –4.87 eV for as-spun films (Figure 1), which were about 0.2–0.4 eV higher than those obtained by cyclic voltammetry (CV), yet the similar variation trend was preserved (Figure S1, SI). Using their optical band gaps, we estimated their lowest unoccupied molecular orbital (LUMO) levels to be in the range of –3.68 to –3.52 eV (Table 1). Note that the tendency of DPP-based polymers to easily form aggregates in the solid state implies that the values obtained for the energy levels cannot be deemed absolute values.[7] On the other hand, computational results (density functional theory (DFT), B3LYP/6–31G*) showed that the HOMOs were well delocalized along the polymer chains but the LUMOs were slightly localized on the DPP core, together with their high degree of structural coplanarity (Figure S2, SI).

2.3. FET Performance

To investigate the charge-transport properties of these materials, bottom-gate top-contact FETs were fabricated using four ε-branched DPP-based polymers as the semiconducting layers. All the polymers exhibited hole-dominant ambipolar transport, most likely due to the well-delocalized HOMO levels and the lower injection barriers for holes with regard to gold electrodes. This is also related to the high off-currents and threshold voltages in the electrical performance, especially for electron conduction. **Figure 2** shows the representative transfer and output curves of optimized FETs based on the drop-cast ε-based DPP polymer films. The typical V-shaped traces in the transfer curves are indicative of ambipolar charge transport. In particular, **PDPP(SE)-ε-C_8C_{15}** and **PDPP(T)-ε-C_8C_{15}** films exhibited remarkably high values of μ_h and μ_e of up to 12.25/2.25 and 8.32/1.26 cm^2 V^{-1} s^{-1}, respectively, in the optimized films annealed at 220°C (**Table 2**). Furthermore, the as-cast **PDPP(SE)-ε-C_8C_{15}** polymer films also showed high ambipolar mobilities of ≈5.57/1.10 cm^2 V^{-1} s^{-1} (Table S1, SI). The superior ambipolar FET performance of **PDPP(SE)-ε-C_8C_{15}** might be attributed to the stronger intermolecular interactions induced by selenium through Se···Se contacts and its lowest band gap with a lower-lying LUMO energy level that facilitated electron injection from gold contact, compared with those of other polymers. Moreover, **PDPP(SE)-ε-C_8C_{15}** exhibited remarkably improved electrical performance in comparison with previously reported PDPP(SE),[3a] presumably due to the positive effects of the extended branching point of alkyl side chains. On the other hand, **PDPP(DT)-ε-C_8C_{15}** and **PDPP(TVT)-ε-C_8C_{15}** exhibited relatively poor ambipolar performance with far more hole-dominant transport. The maximum hole mobilities of 4.36 and 5.20 cm^2 V^{-1} s^{-1} were obtained from the optimized **PDPP(DT)-ε-C_8C_{15}** and **PDPP(TVT)-ε-C_8C_{15}** films, respectively, whereas the electron mobilities were approximately 10–50 times lower than the hole mobilities ($\mu_{e,max}$ ≈ 0.56 cm^2 V^{-1} s^{-1}). The highly π-extended backbone structures with electron-rich groups (DT and TVT) led to higher-lying LUMO energy levels, which might increase electron injection barriers. This is in line with the lowest electron mobilities of **PDPP(TVT)-ε-C_8C_{15}** films. In order to exploit the merit of ambipolar charge transport, complementary metal–oxide–semiconductor (CMOS)-like inverter characteristics were tested using **PDPP(SE)-ε-C_8C_{15}** and **PDPP(T)-ε-C_8C_{15}** films, which exhibited high gains of 61.7 and 51.4, respectively (**Figure 3**). The detrimental effects driven by the asymmetry in mobility and threshold voltage in *p*- and *n*-channel modes may be overcome with further optimization of device architecture. Further experiments are currently underway to improve the inverter characteristics of both polymers and finally realize the high performance organic circuits.

2.4. Thin-Film Microstructure Analysis

To elucidate the observed FET performance in terms of morphological aspects, we investigated the structural features of the polymer films by atomic force microscopy (AFM) analysis (**Figure 4**). The annealed films formed densely packed nanofibrillar structures with interconnected domains that acted as efficient pathways for charge-carrier transport. In particular, for **PDPP(SE)-ε-C_8C_{15}** and **PDPP(T)-ε-C_8C_{15}** films, distinct fibrillar networks were observed over the whole surface area. The **PDPP(SE)-ε-C_8C_{15}** film showed relatively larger fibrils (≈110 nm in diameter) than those of the **PDPP(T)-ε-C_8C_{15}**

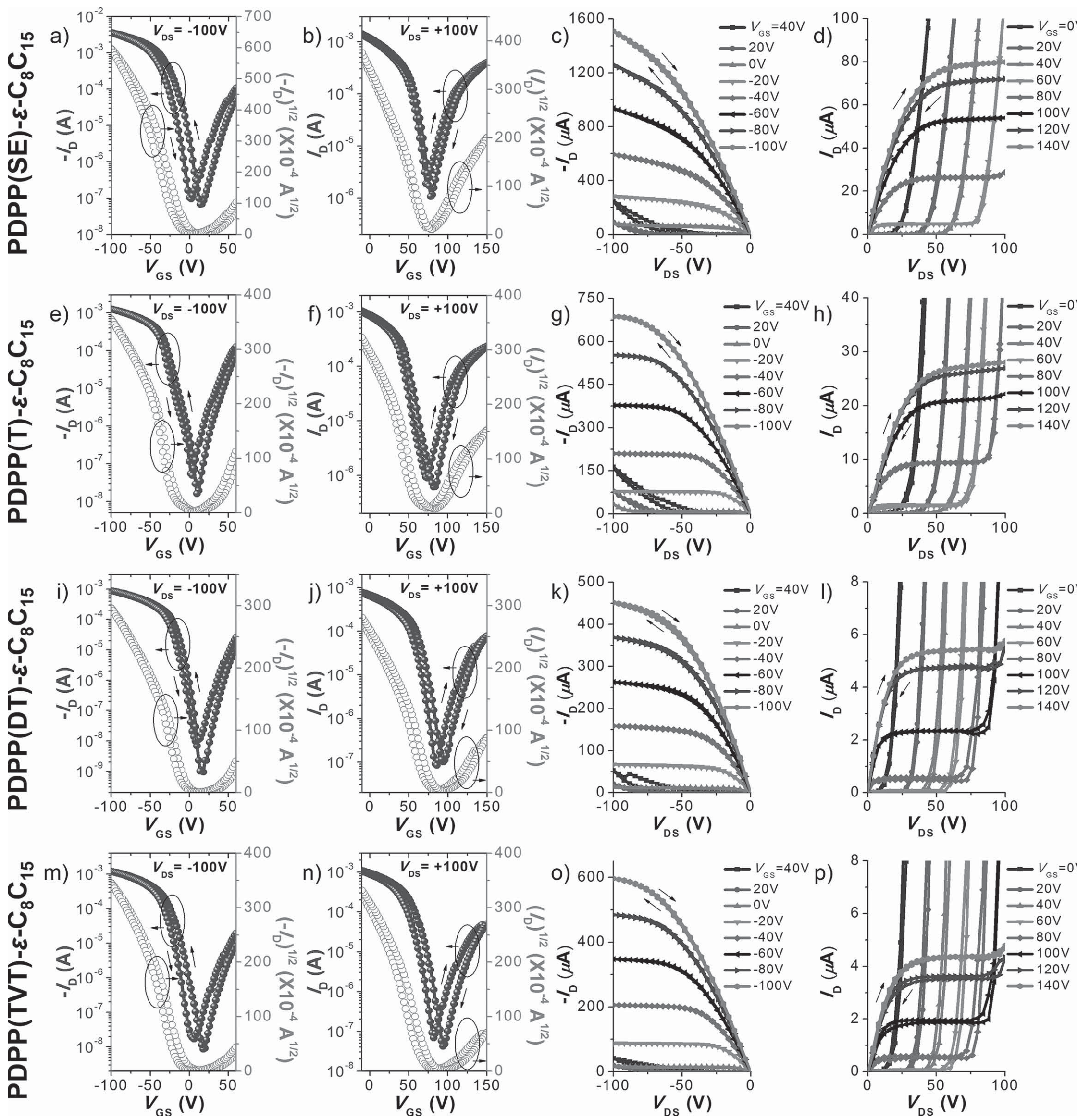

Figure 2. Current–voltage (I–V) curves obtained from FET devices with ε-branched DPP polymer films annealed at 220 °C: a–d) **PDPP(SE)-ε-C_8C_{15}**, e–h) **PDPP(T)-ε-C_8C_{15}**, i–l) **PDPP(DT)-ε-C_8C_{15}**, and m–p) **PDPP(TVT)-ε-C_8C_{15}**. Transfer characteristics at a,e,i,m) hole- and b,f,j,n) electron-enhancement operation with $V_{DS} = -100$ and +100V, respectively. Output characteristics at c,g,k,o) p- and d,h,l,p) n-channel operation (L = 50 μm and W = 1000 μm).

film (≈70 nm), which is closely related to the better charge-transport capability. On the other hand, the **PDPP(DT)-ε-C_8C_{15}** film formed smaller fibrillar domains with some portions of granular structures. The annealed thin films formed enlarged fibrillar structures compared with the as-cast films, illustrating improved FET device performance as compared with the as-cast thin films (Figure S3, SI). However, the **PDPP(TVT)-ε-C_8C_{15}** film exhibited strong intermolecular interactions upon thermal annealing, thus resulting in the creation of crater-like voids with the formation of large aggregates of fibrils (≈350 nm) (Figure S4, SI).

To clarify the crystallinities and molecular orientations of the polymer films further, grazing incidence X-ray diffraction (GIXD) analyses were also performed. **Figure 5** shows the GIXD images and the corresponding diffractogram profiles of the annealed polymer films. The polymers exhibited dominant edge-on orientations with well-defined lamellar peaks up to the fifth order. (**Table 3**) The influence of thermal annealing on the crystallinities of the films was observed in the strongly increased peak intensities and decreased lamellar distances compared with those of the as-cast films (Table S2 and Figure S5, SI). **PDPP(SE)-ε-C_8C_{15}** and **PDPP(T)-ε-C_8C_{15}** had similar lamellar packing structures with only a small difference (≈0.2 Å) in their d-spacings. We further determined the effects of the branching position by comparing the side-chain branching position between the previously reported β-branched chain and the novel ε-branched chain (Figure S6, SI). Compared with thermally annealed β-branched PDPP(SE) films that show diffraction peaks up to the fourth order,[3b] **PDPP(SE)-ε-C_8C_{15}** exhibited higher-order peaks up to the fifth

Table 2. Optimized FET performance of ε-branched DPP polymer films.[a)]

Polymer film[b)]		p-channel				n-channel			
		$\mu_{h,max}$[c)] [cm^2 V^{-1} s^{-1}]	$\mu_{h,avg}$[d)] [cm^2 V^{-1} s^{-1}]	I_{on}/I_{off}[e)]	$V_{T,avg}$ [V]	$\mu_{e,max}$ [cm^2 V^{-1} s^{-1}]	$\mu_{e,avg}$ [cm^2 V^{-1} s^{-1}]	I_{on}/I_{off}	$V_{T,avg}$ [V]
PDPP(SE)-ε-C$_8$C$_{15}$	Spin-coating	6.22	5.64 (±0.46)[f)]	10^6–10^7	−9.3 (±0.9)	1.59	1.15 (±0.17)	10^2–10^4	86.4 (±2.8)
	Drop-casting	12.25	8.25 (±2.47)	10^4–10^6	−9.2 (±2.3)	2.25	1.38 (±0.48)	10^2–10^3	78.0 (±8.2)
PDPP(T)-ε-C$_8$C$_{15}$	Spin-coating	5.81	5.34 (±0.28)	10^4–10^5	−14.6 (±0.7)	0.96	0.79 (±0.09)	10^2–10^3	81.9 (±1.1)
	Drop-casting	8.32	6.06 (±0.99)	10^4–10^6	−13.2 (±3.5)	1.26	0.97 (±0.12)	10^2–10^3	80.6 (±3.9)
PDPP(DT)-ε-C$_8$C$_{15}$	Spin-coating	3.47	3.15 (±0.22)	10^5–10^6	−6.4 (±0.5)	0.39	0.31 (±0.07)	10^2–10^3	97.8 (±4.7)
	Drop-casting	4.36	4.00 (±0.20)	10^5–10^7	−5.5 (±5.1)	0.56	0.34 (±0.09)	10^2–10^4	96.8 (±4.5)
PDPP(TVT)-ε-C$_8$C$_{15}$	Spin-coating	4.34	3.48 (±0.58)	10^5–10^6	−5.5 (±3.4)	0.19	0.13 (±0.05)	10^2–10^3	97.4 (±3.6)
	Drop-casting	5.20	4.48 (±0.43)	10^5–10^7	−4.2 (±1.7)	0.19	0.14 (±0.03)	10^2–10^3	97.1 (±12.7)

[a)]The polymer films were annealed at 220 °C and their FET performance of more than 30 devices was tested in a nitrogen atmosphere; [b)]The device performance of drop-cast films was better than that of spin-coated films, which can be attributed to their highly crystalline nature developed by relatively slow evaporation of solvent; [c)]The maximum and [d)]average mobility of the FET devices (L = 50 µm and W = 1000 µm); [e)]The range of on- and off-current ratio; [f)]The standard deviation.

order, a π–π stacking peak at $q_z \approx 1.72$ Å^{-1}, as well as enhanced crystallinities along the in-plane direction (**Figure 6**). Despite the increased (100) layer distance (by ≈4.1 Å) upon changing the alkyl spacer from methyl to butyl unit, the π–π stacking distance decreased with increasing alkyl spacer length, from 3.96 Å for a β-branched chain to 3.65 Å for a ε-branched chain, which may lead to facilitated 3-D charge transport in **PDPP(SE)-ε-C$_8$C$_{15}$**. This may result from the stronger intermolecular π–π interactions by alleviating the steric side effect of alkyl chains to the conjugated backbone. On the other hand, **PDPP(DT)-ε-C$_8$C$_{15}$** and **PDPP(TVT)-ε-C$_8$C$_{15}$** showed slightly shorter (100) layer distances of 23.92 and 23.36 Å than **PDPP(T)-ε-C$_8$C$_{15}$** (25.97 Å), indicating the more tilted or interdigitated side chains from the extended π-conjugation systems. Although the shorter layer distance may be favorable for the charge transport, the number of layers, estimated from $L_{c(100)}/d_{(100)}$, can reveal more accurate combined effects of layer distance and crystallite size (coherence length of the layer). The $L_{c(100)}/d_{(100)}$ of **PDPP(T)-ε-C$_8$C$_{15}$**, **PDPP(DT)-ε-C$_8$C$_{15}$**, and **PDPP(TVT)-ε-C$_8$C$_{15}$** was estimated to be 9.4, 8.6, and 7.4 layers, respectively. This may account for the relatively lower mobilities of **PDPP(DT)-ε-C$_8$C$_{15}$** and **PDPP(TVT)-ε-C$_8$C$_{15}$**. Furthermore, the homogeneity (structural distribution) of the π–π and lamellar stacking, estimated from the circular averaging of (010) and (100) diffraction peak, can be used to explain the favorable structure for the charge transport. Figure S7 (SI) shows the circular averaging of (010) and (100) peaks of **PDPP(T)-ε-C$_8$C$_{15}$** and **PDPP(DT)-ε-C$_8$C$_{15}$**, where **PDPP(T)-ε-C$_8$C$_{15}$** reveals much narrower distribution both in the π–π and lamellar stacking structures than **PDPP(DT)-ε-C$_8$C$_{15}$**, implying more favorable charge transport for **PDPP(T)-ε-C$_8$C$_{15}$**. All polymer films featured strong perpendicular molecular orientations together with the presence of π–π stacking (π-stack distance ≈3.67 Å) on the substrate. This result suggests that the ε-branched DPP-based polymer films would be able to build up edge-on dominant 3-D conduction channels that would be efficient pathways for charge transport.

3. Conclusion

In summary, the recent interest in tuning the intrinsic properties of semiconducting polymers via side-chain engineering

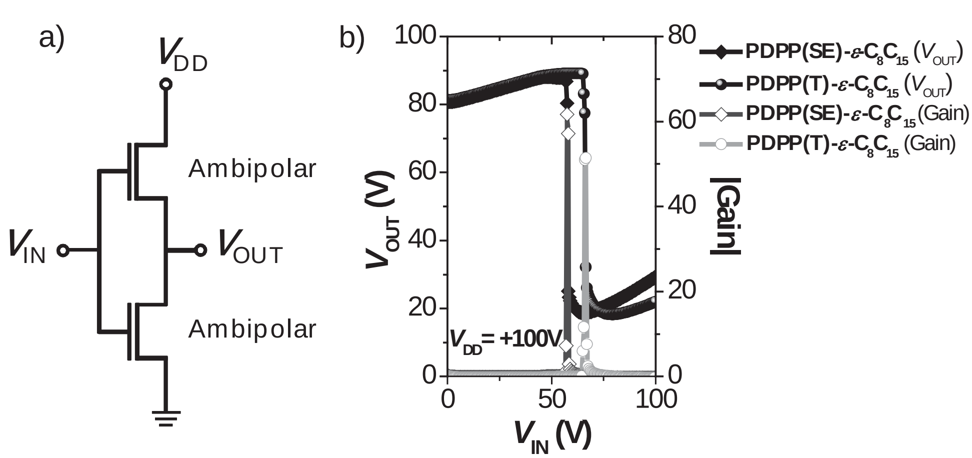

Figure 3. a) Schematic of the complementary inverter structure. b) CMOS-like inverter characteristics of **PDPP(SE)-ε-C$_8$C$_{15}$** and **PDPP(T)-ε-C$_8$C$_{15}$** inverters (V_{DD} = +100 V).

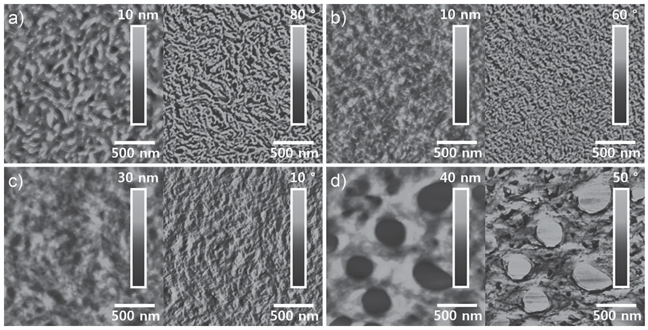

Figure 4. AFM height (left) and phase (right) images of polymer films annealed at 220 °C: a) **PDPP(SE)-ε-C_8C_{15}**, b) **PDPP(T)-ε-C_8C_{15}**, c) **PDPP(DT)-ε-C_8C_{15}**, and d) **PDPP(TVT)-ε-C_8C_{15}**. The polymer films were prepared by drop-casting method on OTS-treated SiO_2/Si substrates.

prompted us to introduce a side-chain modulated branching point—ε-branched position from the backbone—to DPP-based polymers with a view to obtaining high-performance conjugated polymers. We demonstrated that the use of ε-C_8C_{15} solubilizing groups in DPP-based polymers triggers a critical change of polymer chain orientations in thin films, resulting in a dramatic improvement in FET devices (μ_h up to 12.25 cm^2 V^{-1} s^{-1} and $I_{on}/I_{off} \geq 10^6$ while maintaining their good electron mobilities). Not only do the vastly superior FET performance characteristics represent a significant achievement in organic semiconductor development, but also the applicability of the branching point platform extends beyond the examples studied here, which will help propel the development of other disciplines.

4. Experimental Section

Materials and Instruments: All the chemicals and reagents were bought from Sigma-Aldrich, Alfa Aesar chemical company, Tokyo Chemical Industry Co., Ltd. and unless otherwise specified used without any further purification. THF was freshly dried over sodium and benzophenone, prior to use. ^{1}H and ^{13}C NMR spectra were recorded on a Varian VNRS 600 MHz spectrometer using deuterated chloroform ($CDCl_3$) or 1,1,2,2-tetrachloroethane $C_2D_2Cl_4$) as solvent. The chemical shifts were given in parts per million and coupling constants (*J*) in Hertz. The elemental analysis of carbon, hydrogen, nitrogen, and sulphur were carried out with a Flesh 2000 elemental analyser. MALDI-MS spectra were recorded by Ultraflex III (Bruker). UV–Vis–NIR spectra were taken on Cary 5000 (Varian USA) spectrophotometer. The molecular weight of the polymers were determined by gel-permeation chromatography (GPC) with at 150 °C on a Varian system using a PL gel mixed-B column and 1,2,4-trichlorobenzene as eluent. The electrochemical properties were characterized by VersaSTAT3 Princeton Applied Research Potentiostat with platinum as working electrode, a platinum wire counter electrode, and Ag/Ag$^+$ as reference electrode. The electrolytic solution employed

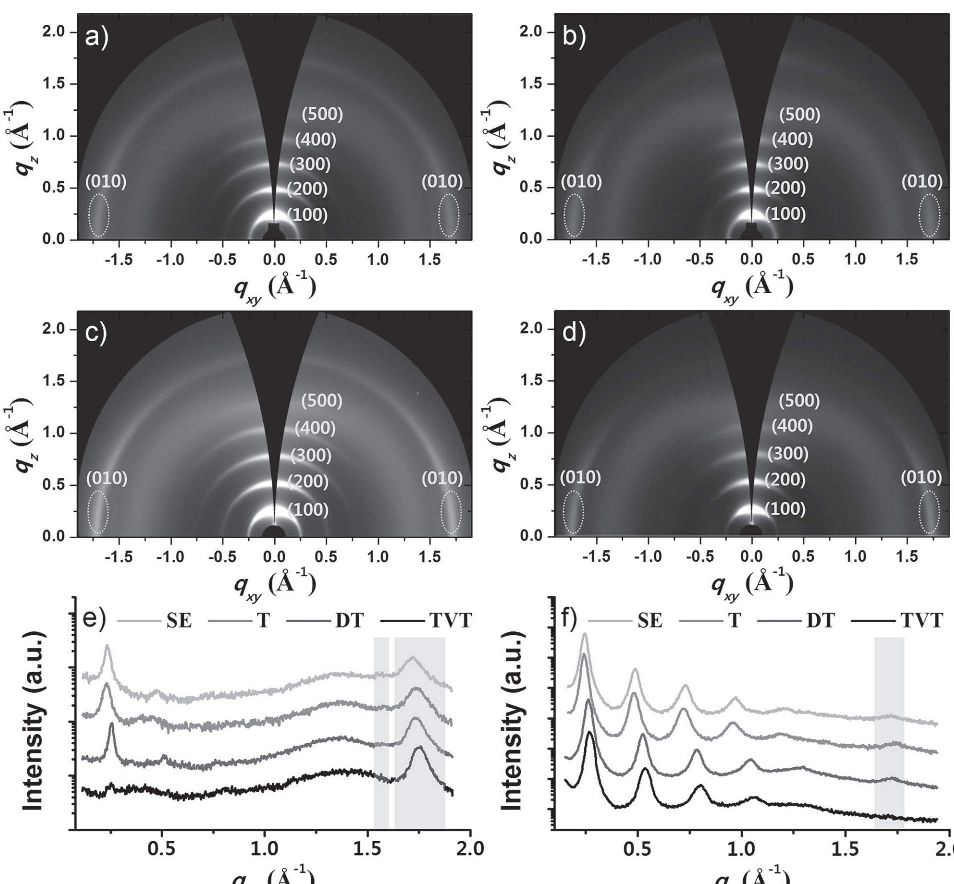

Figure 5. 2D-GIXD images of polymer films annealed at 220 °C: a) **PDPP(SE)-ε-C_8C_{15}**, b) **PDPP(T)-ε-C_8C_{15}**, c) **PDPP(DT)-ε-C_8C_{15}**, and d) **PDPP(TVT)-ε-C_8C_{15}**. The corresponding GIXD diffractogram profiles: e) in-plane and f) out-of-plane GIXD patterns. The polymer films were prepared by drop-casting method on OTS-treated SiO_2/Si substrates.

Table 3. Crystallographic parameters of optimized ε-branched DPP polymer films.[a)]

Polymer	Lamellar spacing					π–π spacing		
	q_z [Å^{-1}]	d [Å]	FWHM [Å^{-1}]	L_c [Å]	q_{xy} [Å^{-1}]	d [Å]	q_z [Å^{-1}]	d [Å]
PDPP(SE)-ε-C$_8$C$_{15}$	0.244	25.73	0.0256	220.7	1.720	3.65	1.721	3.65
PDPP(T)-ε-C$_8$C$_{15}$	0.242	25.97	0.0232	243.7	1.736	3.62	1.745	3.60
PDPP(DT)-ε-C$_8$C$_{15}$	0.263	23.92	0.0276	204.8	1.736	3.62	1.726	3.65
PDPP(TVT)-ε-C$_8$C$_{15}$	0.269	23.36	0.0329	172.1	1.752	3.59	1.712[b)]	3.67

[a)]The polymer films were prepared by drop-casting and thermal treatment at 220 °C, and their parameters were calculated from GIXD profiles. All polymer films exhibited minor peak at $q_{xy} \approx 1.58$ Å^{-1}, corresponding to the alkyl chain interactions of ε-branched chains with d-spacing of about ≈4 Å; [b)]For **PDPP(TVT)-ε-C$_8$C$_{15}$** films, the relatively weak π–π stacking was observed in out-of-plane GIXD patterns.

were 0.1 M tetra-n-butylammonium hexafluorophosphate (n-Bu$_4$NPF$_6$) in dry acetonitrile at a scan rate of 100 mV/s under Ar atmosphere. The reference electrode was calibrated using a ferrocene/ferrocenium redox couple as external standard, whose oxidation potential is set at –4.8 eV with respect to zero vacuum level. The HOMO energy levels of the polymers were obtained from the equation:

$$E_{\mathrm{HOMO}}(\mathrm{eV}) = -\left(E^{\mathrm{onset}}_{(\mathrm{ox})} - E^{\mathrm{onset}}_{(\mathrm{ferrocene})} + 4.8\right) \tag{1}$$

and the corresponding LUMO levels were calculated by using equation :

$$E_{\mathrm{LUMO}}(\mathrm{eV}) = -\left(E^{\mathrm{onset}}_{(\mathrm{red})} - E^{\mathrm{onset}}_{(\mathrm{ferrocene})} + 4.8\right) \tag{2}$$

Tapping-mode atomic force microscopy (AFM) measurements were performed using an Agilent 5500 scanning probe microscope (SPM) running with a Nanoscope-V controller. Grazing incidence X-ray diffraction (GIXD) measurements were conducted at PLS-II 9A U-SAXS beamline of Pohang Accelerator Laboratory in Korea. The X-rays coming from the in-vacuum undulator (IVU) were monochromated at 11.17 keV (wavelength, λ = 1.1099 Å) using a double crystal monochromator, and focused both horizontally and vertically (450 μm (H) × 60 μm (V) in FWHM @ sample position) using K-B type mirrors. GIXD sample stage was equipped with a 7-axis motorized stage for the fine alignment of sample and the incidence angle of X-ray beam was set to in the range of 0.11°, which was close to the critical angle of samples. GIXD patterns were recorded with a 2D CCD detector (Rayonix SX165) and X-ray irradiation time was ranged from 30 s to 60 s, depending on the saturation level of the detector. Diffraction angles were calibrated using a pre-calibrated sucrose (Monoclinic, P21, a = 10.8631 Å, b = 8.7044 Å, c = 7.7624 Å, b = 102.938°) and the sample-to-detector distance was ≈224.4 mm.

General Procedure for Polymerization and Polymer Purification: 3,6-bis(5-bromothiophen-2-yl)-2,5-bis(5-octylpentadecyl)-2,5-dihydropyrrolo[3,4-c]pyrrole-1,4-dione (**1**) (0.250 mmol) and distannyl compound (0.250 mmol) were taken in a Schlenk tube under argon atmosphere with 10 mL of anhydrous chlorobenzene. The mixture was degassed for 20 min followed by addition of Pd$_2$(dba)$_3$ (8 mg, 8.7 μmol) and P(o-tolyl)$_3$ (13 mg, 42 μmol) for polymer **PDPP(SE)-ε-C$_8$C$_{15}$** and **PDPP(T)-ε-C$_8$C$_{15}$**. Note that in the cases of **PDPP(DT)-ε-C$_8$C$_{15}$** and **PDPP(TVT)-ε-C$_8$C$_{15}$**, Pd(PPh$_3$)$_4$ (6 mg) as the catalyst was applied, respectively, since the polymerization mixture gelated within 30 min to 1 h under Pd$_2$(dba)$_3$/P(o-tolyl)$_3$. The mixture was heated at 110 °C for 24 h. After cooling to room temperature, it was poured into methanol and the resulting precipitate was filtered. The polymer was purified by Soxhlet extraction using methanol, acetone, and hexane, and finally extracted with monochlorobenzene. The monochlorobenzene solution was then concentrated by evaporation and re-precipitated in methanol. The resulting dark solid was collected and dried overnight under vacuum. The polymers were characterized by ^{1}H NMR, GPC, and elemental analysis. Synthesis and characterization of the intermidiates for the polymers are detailed in the Supporting Information.

PDPP(SE)-ε-C$_8$C$_{15}$: Isolated yield = 95%. GPC analysis (temperature 150 °C) M_n = 38,253 Da, M_w = 98,465 Da, and PDI = 2.57 (against PS standard).^{1}H NMR (C$_2$D$_2$Cl$_4$, 600 MHz, 353 K): δ ppm 8.96 (br, 2H), 7.35–6.68 (br, 4H), 4.14 (br, 4H), 1.95–1.13 (br, 78H), 0.93 (br, 12H). Anal.calc. for: C$_{64}$H$_{102}$N$_2$O$_2$S$_2$Se: C, 71.53; H, 9.57; N, 2.61; S, 5.97; found: C, 70.89; H, 9.20; N, 2.46; S, 5.73.

PDPP(T)-ε-C$_8$C$_{15}$: Isolated yield = 97%. GPC analysis (temperature 150 °C) M_n = 50,862 Da, M_w = 115,885 Da, and PDI = 2.28 (against PS standard).^{1}H NMR (C$_2$D$_2$Cl$_4$, 600 MHz, 353 K): δ ppm 8.94 (br, 2H), 7.34–6.68 (br, 4H), 4.14 (br, 4H), 1.97–1.13 (br, 78 H), 0.93 (br, 12H). Anal.calc. for C$_{64}$H$_{102}$N$_2$O$_2$S$_3$: C, 74.80; H, 10.00; N, 2.73; S, 9.36; Found: C, 74.19; H, 9.65; N, 2.61; S, 8.88.

PDPP(DT)-ε-C$_8$C$_{15}$: Isolated yield = 60%. GPC analysis (temperature 150 °C) M_n = 15,428 Da, M_w = 30,003 Da, and PDI = 1.95 (against PS standard). ^{1}H NMR (C$_2$D$_2$Cl$_4$, 600 MHz, 353 K): δ ppm 8.91 (br, 2H), 7.47–6.66 (br, 6H), 4.12 (br, 4H), 1.94–1.13 (br, 78 H), 0.94 (br, 12H). Anal.calc. for C$_{68}$H$_{104}$N$_2$O$_2$S$_4$: C, 73.59; H, 9.45; N, 2.52; S, 11.55; found: C, 73.59; H, 9.23; N, 2.42; S, 11.19.

PDPP(TVT)-ε-C$_8$C$_{15}$: Isolated yield = 52%. GPC analysis (temperature 150 °C) M_n = 19,015 Da, M_w = 39,217 Da, and PDI = 2.06 (against PS standard).^{1}H NMR (C$_2$D$_2$Cl$_4$, 600 MHz, 353 K): δ ppm 8.91 (br, 2H), 7.46–6.47 (br, 8 H), 4.07 (br, 4H), 1.93–1.17 (br, 78 H,), 0.93 (br, 12H). Anal.calc. for C$_{70}$H$_{106}$N$_2$O$_2$S$_4$: C, 74.02; H, 9.41; N, 2.47; S, 11.29; found: C, 73.66; H, 9.36; N, 2.32; S, 10.72.

FET Fabrication and Measurement: FETs with bottom-gate top-contact configuration were prepared to characterize the electrical performance of ε-branched DPP polymers. A highly n-doped (100) Si wafer (<0.004 Ω cm) with a thermally grown SiO$_2$ (300 nm, C_i = 10 nF cm^{-2}) was utilized as the substrate and gate dielectrics and the SiO$_2$ surface

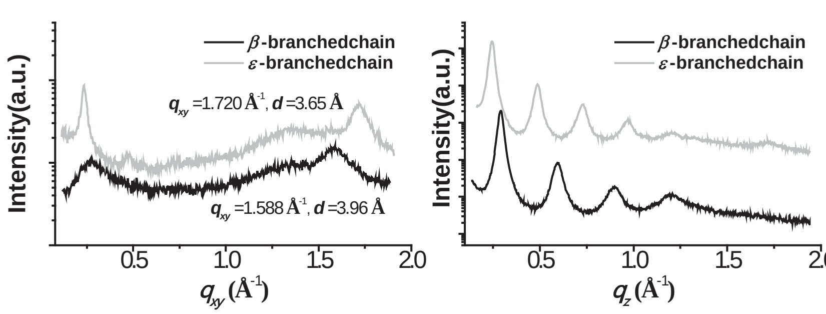

Figure 6. Comparison of GIXD diffractogram profiles of PDPP(SE) films with different branched side-chain: β- and ε-branching position. In-plane (left) and out-of-plane (right) GIXD patterns of the polymer films annealed at 220 °C. The polymer films were prepared by drop-casting method on OTS-treated SiO$_2$/Si substrates.

was modified with *n*-octadecyltrimethoxysilane (OTS) as self-assembled monolayer (SAM) according to previously reported method. 3 mM of OTS solution in trichloroethylene was spin-coated on the piranha-treated wafer at 3000 rpm for 30 s. Then, the wafer was exposed to ammonia vapor for ≈12 h to facilitate the formation of SAM, followed by sonication cleaning, sequential washing, and drying. The contact angle (droplet of DI water) on the hydrophobic OTS-modified wafer was ≈110°. The ε-branched DPP polymers were dissolved in anhydrous chlorobenzene (3 mg mL^{-1}) and the polymer film was drop-cast onto the substrate. Au contacts (40 nm) were thermally evaporated onto the polymer films to form source and drain electrodes with a channel length (L) of 50 µm and a width (W) of 1000 µm using a shadow mask. The electrical performance of FETs was tested in N_2 atmosphere using a Keithley 4200 semiconductor parametric analyzer. The field-effect mobility was calculated in the saturation regime using the following equation:

$$I_{DS} = 1/2(W/L)\mu C_i(V_G - V_T)^2 \quad (3)$$

where I_{DS} is the drain-to-source current, μ is the mobility, and V_G and V_T are the gate voltage and threshold voltage, respectively.

Supporting Information

Supporting Information is available from the Wiley Online Library or from the author.

Acknowledgements

A-R.H., G.K.D., and J.L. contributed equally to the work. This work was supported by the National Research Foundation of Korea (NRF) funded by the Ministry of Education (2013R1A1A1A05004475, 2010–0019408, 2014R1A2A2A01007467, BK21 Plus), Global Frontier Research Program of Ministry of Science, ICT and Future Planning (2013M3A6A5073175).

Received: September 1, 2014
Revised: October 24, 2014
Published online: November 20, 2014

[1] a) A. N. Sokolov, B. C.-K. Tee, C. J. Bettinger, J. B.-H. Tok, Z. Bao, *Acc. Chem. Res.* **2011**, *45*, 361; b) Z. Chen, M. J. Lee, R. S. Ashraf, Y. Gu, S. Albert-Seifried, M. Meedom Nielsen, B. Schroeder, T. D. Anthopoulos, M. Heeney, I. McCulloch, H. Sirringhaus, *Adv. Mater.* **2012**, *24*, 647; c) H. Zhang, X. Guo, J. Hui, S. Hu, W. Xu, D. Zhu, *Nano Lett.* **2011**, *11*, 4939; d) S. C. B. Mannsfeld, B. C.-K. Tee, R. M. Stoltenberg, C. V. H.-H. Chen, S. Barman, B. V. O. Muir, A. N. Sokolov, C. Reese, Z. Bao, *Nat. Mater.* **2010**, *9*, 859; e) G. H. Gelinck, H. E. A. Huitema, E. van Veenendaal, E. Cantatore, L. Schrijnemakers, J. B. P. H. van der Putten, T. C. T. Geuns, M. Beenhakkers, J. B. Giesbers, B.-H. Huisman, E. J. Meijer, E. M. Benito, F. J. Touwslager, A. W. Marsman, B. J. E. van Rens, D. M. de Leeuw, *Nat. Mater.* **2004**, *3*, 106.
[2] a) H. Chen, Y. Guo, G. Yu, Y. Zhao, J. Zhang, D. Gao, H. Liu, Y. Liu, *Adv. Mater.* **2012**, *24*, 4618; b) A. Facchetti, *Chem. Mater.* **2010**, *23*, 733; c) W. Zhang, J. Smith, S. E. Watkins, R. Gysel, M. McGehee, A. Salleo, J. Kirkpatrick, S. Ashraf, T. Anthopoulos, M. Heeney, I. McCulloch, *J. Am. Chem. Soc.* **2010**, *132*, 11437; d) H. Bronstein, Z. Chen, R. S. Ashraf, W. Zhang, J. Du, J. R. Durrant, P. Shakya Tuladhar, K. Song, S. E. Watkins, Y. Geerts, M. M. Wienk, R. A. J. Janssen, T. Anthopoulos, H. Sirringhaus, M. Heeney, I. McCulloch, *J. Am. Chem. Soc.* **2011**, *133*, 3272; e) J. Mei, D. H. Kim, A. L. Ayzner, M. F. Toney, Z. Bao, *J. Am. Chem. Soc.* **2011**, *133*, 20130; f) H. N. Tsao, D. M. Cho, I. Park, M. R. Hansen, A. Mavrinskiy, D. Y. Yoon, R. Graf, W. Pisula, H. W. Spiess, K. Müllen, *J. Am. Chem. Soc.* **2011**, *133*, 2605; g) M. J. Cho, J. Shin, S. H. Yoon, T. W. Lee, M. Kaur, D. H. Choi, *Chem. Commun.* **2013**, *49*, 7132.
[3] a) J. Lee, A.-R. Han, J. Kim, Y. Kim, J. H. Oh, C. Yang, *J. Am. Chem. Soc* **2012**, *134*, 20713; b) J. Lee, A.-R. Han, H. Yu, T. J. Shin, C. Yang, J. H. Oh, *J. Am. Chem. Soc.* **2013**, *135*, 9540; c) I. Kang, H.-J. Yun, D. S. Chung, S.-K. Kwon, Y.-H. Kim, *J. Am. Chem. Soc.* **2013**, *135*, 14896; d) I. Kang, T. K. An, J.-a. Hong, H.-J. Yun, R. Kim, D. S. Chung, C. E. Park, Y.-H. Kim, S.-K. Kwon, *Adv. Mater.* **2013**, *25*, 524; e) J. Li, Y. Zhao, H. S. Tan, Y. Guo, C.-A. Di, G. Yu, Y. Liu, M. Lin, S. H. Lim, Y. Zhou, H. Su, B. S. Ong, *Sci. Rep.* **2012**, *2*, f) Y. Li, P. Sonar, L. Murphy, W. Hong, *Energy Environ. Sci.* **2013**, *6*, 1684.
[4] B. Fu, J. Baltazar, A. R. Sankar, P.-H. Chu, S. Zhang, D. M. Collard, E. Reichmanis, *Adv. Funct. Mater.* **2014**, *24*, 3734.
[5] M. Jung, Y. Yoon, J. H. Park, W. Cha, A. Kim, J. Kang, S. Gautam, D. Seo, J. H. Cho, H. Kim, J. Y. Choi, K. H. Chae, K. Kwak, H. J. Son, M. J. Ko, H. Kim, D.-K. Lee, J. Y. Kim, D. H. Choi, B. S. Kim, *ACS Nano* **2014**, *8*, 5988.
[6] a) Y. Kim, J. Hong, J. H. Oh, C. Yang, *Chem. Mater.* **2013**, *25*, 3251; b) J. S. Ha, K. H. Kim, D. H. Choi, *J. Am. Chem. Soc.* **2011**, *133*, 10364; c) B. Lim, K.-J. Baeg, H.-G. Jeong, J. Jo, H. Kim, J.-W. Park, Y.-Y. Noh, D. Vak, J.-H. Park, J.-W. Park, D.-Y. Kim, *Adv. Mater.* **2009**, *21*, 2808.
[7] R. S. Ashraf, A. J. Kronemeijer, D. I. James, H. Sirringhaus, I. McCulloch, *Chem. Commun.* **2012**, *48*, 3939.